


# SCIENTIFIC REPORTS

OPEN

## Structure and dynamics in the lithium solvation shell of nonaqueous electrolytes

Sungho Han 

The solvation of a lithium ion has been of great importance to understand the structure and dynamics of electrolytes. In mixed electrolytes of cyclic and linear carbonates, the lithium solvation structure and the exchange dynamics of solvents strongly depend on the mixture ratio of solvents, providing a connection of the rigidity of the lithium solvation shell with the solvent composition in the shell. Here we study the dynamical properties of solvents in the solvation sheath of a lithium ion for various solvent mixture ratios via molecular dynamics simulations. Our results demonstrate that the exchange dynamics of solvents exhibits a non-monotonic behavior with a change in the mixture ratio, which keeps preserved on both short and long time scales. As the fraction of cyclic carbonate increases, we find that the structural properties of cyclic and linear carbonates binding to a lithium ion show different responses to a change in the fraction. Furthermore, we find that the rotational dynamics of cyclic carbonate is relatively insensitive to the mixture ratio in contrast to the rotational dynamics of linear carbonate. Our results further present that an anion shows different properties in structure and dynamics from solvents upon changing the mixture ratio of solvents.

An electrolyte is one of indispensable components of lithium ion batteries<sup>1–5</sup>. It serves as media for lithium ions to move back and forth between cathode and anode during charging and discharging operations<sup>1,5</sup>. The properties required for being good electrolytes of lithium ion batteries includes the good solubility of salt, the good fluidity for the ionic transport and the good stability from any reactions during the battery operation. However, one solvent type in nonaqueous electrolytes cannot satisfy all requirements of electrolytes. Generally, solvents with high dielectric constants present the good solubility of salt but they invoke the high viscosity of electrolytes due to their polar nature, generating the slow transport of Li<sup>+</sup> ions. For solvents with low dielectric constants, on the other hand, they provide the good environments for the fast transport of ions but easily induce the undesirable ion-pairing of cations and anions due to their low solubility. For commercial lithium ion batteries, as a result, the mixed electrolytes consisting of cyclic and linear carbonates such as ethylene carbonate (EC) and dimethyl carbonate (DMC) have generally been used to enhance both the solubility of salt and the mobility of ions, simultaneously. If the fraction of cyclic carbonate in the electrolyte increases, the solubility will also increase but the mobility of ions will undesirably decrease in general. In contrast, if the fraction of linear carbonate increases, the mobility of ions will be improved but the solubility will be worse. In the mixed electrolytes, thus, finding an optimal mixture ratio of solvents has been of great interest to improve the performance of lithium ion batteries.

For the mixed electrolytes of lithium ion batteries, it has been long believed that solvents with high and low dielectric constants, such as EC ( $\epsilon \sim 90$  at 40 °C) and DMC ( $\epsilon \sim 3.1$  at 25 °C), play distinct roles in the electrolyte<sup>1</sup>. Preferentially, EC participates in solvating a Li<sup>+</sup> ion and contributes to form lithium-solvents complexes<sup>6,7</sup>. On the other hand, DMC serves as media for the Li<sup>+</sup> ion-solvents complexes to transport in the electrolyte. Recently, however, many studies have shown that both types of solvents are able to actively participate in forming the lithium solvation sheath and the main factor to determine the composition of the lithium solvation shell is simply the mixture ratio between them, although their dielectric constants show a large difference in magnitude<sup>8–15</sup>. The structure of the lithium solvation sheath has been considered to be crucial for forming the protective film on the electrodes, known as a solid electrolyte interphase (SEI), because the solvents in the solvation sheath predominantly participate in forming the SEI by decomposition<sup>16–18</sup>. The mixture ratio of binary solvents further affect the ionic conductivity, showing a non-monotonic dependence of the ionic conductivity on the mixture ratio

CAE Group, AMD Lab, AI&SW Research Center, Samsung Advanced Institute of Technology, Suwon, Gyeonggi, 16678, Korea. Correspondence and requests for materials should be addressed to S.H. (email: [hellosungho@gmail.com](mailto:hellosungho@gmail.com))

of solvents<sup>1,19</sup>. The non-monotonic behavior in the ionic conductivity is ascribed to a competition between the viscosity of the electrolyte and the ion-pairing of cations and anions. This non-monotonic behavior of the ionic conductivity has also been found in its dependence on the salt concentration<sup>1,19</sup>.

Generally, one considers the rigidity of the solvation shell of ions in electrolytes to be critical for the mobility of ions<sup>20–26</sup>. As the rigidity of the solvation shell increases, the ionic transport slows down due to an increase in the drag against the motion of lithium-solvents complexes<sup>15</sup>. The rigidity of the solvation shell can be characterized by the measure of the residence time of solvents within the solvation shell, which presents how easily the solvation structure can be broken. Hence, the rigidity of the solvation shell is closely related with the exchange dynamics of solvents in the solvation shell – in other words, how long the solvents can reside in the solvation shell<sup>15,26–28</sup>. The faster exchange dynamics of solvents invokes the weaker rigidity of the solvation shell due to the weaker bonding with a Li<sup>+</sup> ion. Obviously, the solvation dynamics has a close connection with the structure of the lithium solvation shell<sup>15</sup>. Since the solvation structure depends on the mixture ratio of solvents, the solvation dynamics would be affected by the mixture ratio as well. Thus, finding the relation between the solvation dynamics and the mixture ratio of solvents would be of significance to broaden our understanding of electrolytes and design them suitable for the future lithium ion batteries.

In this work, we investigate the dynamics in the lithium solvation shell of nonaqueous electrolytes consisting of 1 M lithium hexafluorophosphate (LiPF<sub>6</sub>) with binary solvents of EC and DMC as a function of the solvent mixture ratio at the temperature of  $T = 300$  K. We examine the six different mixture ratios from EC:DMC = 10%:90% up to 60%:40%. For simplicity, we will denote the mixture ratio of binary solvents as only the EC fraction,  $\chi_{EC}$ , throughout this work.

## Results and Discussion

**Solvation dynamics in the lithium solvation shell.** First, we consider how long solvents are able to reside in the first solvation shell of a Li<sup>+</sup> ion as a function of  $\chi_{EC}$ . For the sake of it, we examine the slow and fast solvation dynamics of solvents in the first solvation shell of a Li<sup>+</sup> ion. The reason we consider two different solvation dynamics is that they occur on different time scales and they are based on the different underlying mechanisms<sup>15,28</sup>. First of all, we define the first solvation shell of a Li<sup>+</sup> ion as the first plateau in the cumulative coordination number  $n(r)$ <sup>15,28</sup>, as we will see later. In this definition, the first solvation shell of a Li<sup>+</sup> ion is defined as a circle centered at a Li<sup>+</sup> ion with a radius of 0.3 nm for a carbonyl oxygen atom O<sub>c</sub> of EC and DMC and a circle with a radius of 0.45 nm for a central P atom of a PF<sub>6</sub><sup>-</sup> ion<sup>15</sup>. For the fast solvation dynamics, we define the residence time distribution  $R(t)$  as<sup>15,28–30</sup>

$$R(t) \equiv \langle \Theta(t_b - t) \rangle, \quad (1)$$

where  $\Theta(t)$  is the Heaviside step function,  $t_b$  is the first-passage time for a solvent to be dissociated from the lithium solvation shell and  $\langle \dots \rangle$  represents an ensemble average. In this definition of  $R(t)$ , we consider only the intact bonding of a solvent with a Li<sup>+</sup> ion for a given time interval. The fast solvation dynamics is known to be closely related with the motions occurred on a short time scale, such as the thermal fluctuation<sup>15,28,31</sup>. In Fig. 1(a), we present  $R(t)$  of EC, DMC, and PF<sub>6</sub><sup>-</sup> as a function of time  $t$  at the EC fraction of  $\chi_{EC} = 30\%$ . It shows that  $R_{DMC}(t)$  decays faster than  $R_{EC}(t)$ <sup>32</sup> and  $R_{PF_6^-}(t)$  decays much slower than both  $R_{EC}(t)$  and  $R_{DMC}(t)$ . It indicates that by the thermal fluctuation the two solvents can escape the lithium solvation shell much faster than an anion due to the strong Coulombic interaction of the anion with a cation. As for both solvents, DMC forms the weaker bonding with a Li<sup>+</sup> ion than EC, so that  $R_{DMC}(t)$  decays faster than  $R_{EC}(t)$ <sup>15,32</sup>. Note that those decaying behaviors on a short time scale are valid for all  $\chi_{EC}$ s we investigated.

To characterize the temporal behavior of  $R(t)$  in terms of a single value, we define the characteristic residence time  $\tau_R$  as the time required for  $R(t)$  to decay by a factor of  $e$ <sup>15,28,30</sup>. In Fig. 1(b–d), we present  $\tau_R$  of PF<sub>6</sub><sup>-</sup>, EC and DMC as a function of  $\chi_{EC}$ . Our results show that the exchange dynamics of EC and DMC occurs on the time scale of tens of picoseconds, whereas the exchange dynamics of PF<sub>6</sub><sup>-</sup> occurs in a few nanoseconds. The direct observations on the solvation dynamics have been limited by the experimental difficulties due to the nature of ultrafast dynamics. However, a recent experiment using the coherent two-dimensional infrared spectroscopy has shown that the residence of a solvent in the solvation shell of a Li<sup>+</sup> ion has indeed a finite lifetime and the fast solvation dynamics occurs on the time scale of tens of picoseconds<sup>31</sup>. Our results of the fast solvation dynamics in tens of picoseconds are in good agreement with the experimental results<sup>31</sup>. The behaviors of  $\tau_R^{EC}$  and  $\tau_R^{DMC}$  in terms of  $\chi_{EC}$  are quite different from  $\tau_R^{PF_6^-}$  which decreases monotonically with the increasing  $\chi_{EC}$ . We find that both  $\tau_R^{EC}$  and  $\tau_R^{DMC}$  exhibit non-monotonic behaviors as a function of  $\chi_{EC}$ . As  $\chi_{EC}$  increases to 30%, both  $\tau_R^{EC}$  and  $\tau_R^{DMC}$  decrease the same as in  $\tau_R^{PF_6^-}$ . When  $\chi_{EC}$  further increases, however, we find that  $\tau_R^{EC}$  and  $\tau_R^{DMC}$  now increase, showing the minimum in  $\tau_R^{EC}$  and  $\tau_R^{DMC}$  between  $\chi_{EC} = 30\%$  and 40%.

We further find the similar non-monotonic behaviors in the slow solvation dynamics in terms of  $\chi_{EC}$ . We describe the slow solvation dynamics using the residence correlation time distribution  $C(t)$  defined as<sup>15,28,30</sup>

$$C(t) \equiv \frac{\langle h(t) \cdot h(0) \rangle}{\langle h(0) \cdot h(0) \rangle}, \quad (2)$$

where  $h(t)$  is unity when a solvent is within the first solvation shell of a Li<sup>+</sup> ion and  $h(t)$  is zero, otherwise.  $C(t)$  indicates the conditional probability that a bonding with a Li<sup>+</sup> ion remains intact at time  $t$ , given it was intact at time  $t = 0$ . In contrast to  $R(t)$ ,  $C(t)$  does not consider any breaking of the bond at intermittent times between time  $t = 0$  and  $t$ .  $C(t)$  is closely connected with the motions on a long time scale, such as the diffusive motions. In the inset of Fig. 2(a), we present  $C(t)$  of EC and DMC at the EC fraction of  $\chi_{EC} = 30\%$ .  $C_{EC}(t)$  decays slower than  $C_{DMC}(t)$ , indicating the slower diffusion of EC than DMC. To characterize the temporal behavior of  $C(t)$  in terms

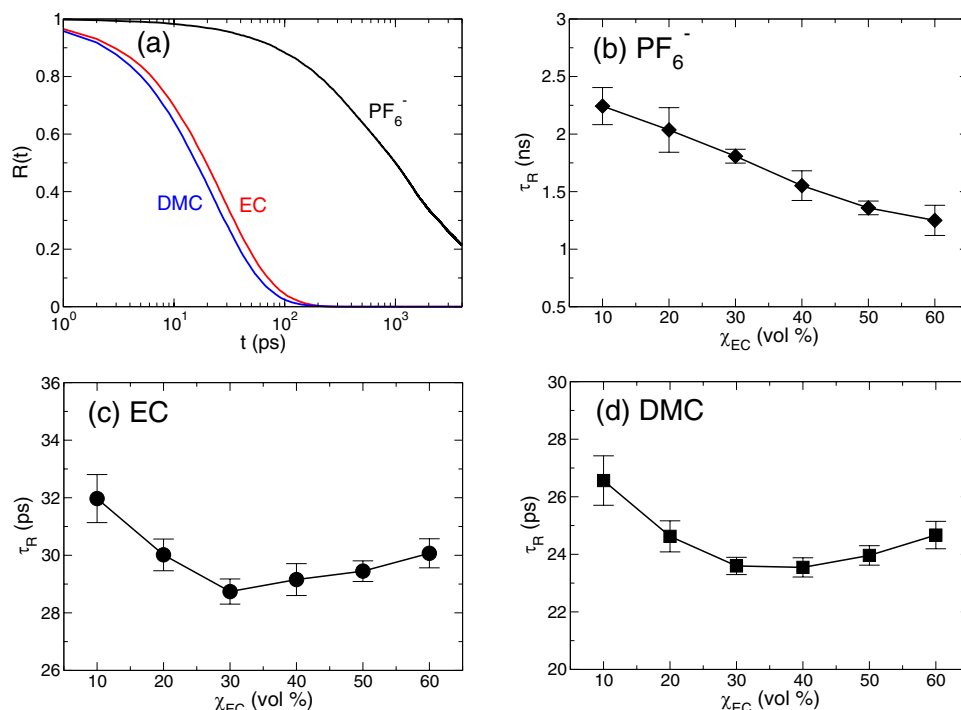


**Figure 1.** The exchange dynamics in the lithium solvation shell on a short time scale. **(a)** The residence time distributions  $R(t)$  of a  $\text{PF}_6^-$  ion, EC and DMC as a function of time  $t$  for the EC fraction of  $\chi_{\text{EC}} = 30\%$ . Next, shown is the characteristic residence time  $\tau_R$  of **(b)**  $\text{PF}_6^-$ , **(c)** EC and **(d)** DMC as a function of  $\chi_{\text{EC}}$ . Whereas  $\tau_R^{\text{PF}_6^-}$  monotonically decreases with increasing  $\chi_{\text{EC}}$ ,  $\tau_R$  for the two solvents, EC and DMC, exhibits a non-monotonic behavior with respect to  $\chi_{\text{EC}}$ . It shows a minimum around the value of  $\chi_{\text{EC}}$  between 30% and 40%.

of a single value, we also define the characteristic correlation time  $\tau_C$  in the same way as in  $\tau_R$ . In Fig. 2, we present  $\tau_C^{\text{EC}}$  and  $\tau_C^{\text{DMC}}$  as a function of  $\chi_{\text{EC}}$ . We find that  $\tau_C^{\text{EC}}$  and  $\tau_C^{\text{DMC}}$  exhibit the same non-monotonic behaviors as in  $\tau_R^{\text{EC}}$  and  $\tau_R^{\text{DMC}}$  with respect to  $\chi_{\text{EC}}$ . It indicates that the dynamic characteristic features of the solvation dynamics on a short time scale keep preserved on a long time scale. Both  $\tau_C^{\text{EC}}$  and  $\tau_C^{\text{DMC}}$  exhibit the minimum around at  $\chi_{\text{EC}} = 30\%$ .

The non-monotonic exchange dynamics of solvents is ascribed to various and complex factors such as the composition of solvents in the lithium solvation shell, an intensity of the bonding of solvents with a  $\text{Li}^+$  ion, the translational and rotational motions of solvents, the interaction between solvents within the lithium solvation shell, the interaction between solvents inside and outside the solvation shell and the position of solvents in the solvation shell, etc. Investigation of only one or two factors might be insufficient to reveal the full underlying mechanism for the non-monotonic exchange dynamics. In despite of it, however, it would be worthy of exploring how some of the factors described the above would be connected with the solvation dynamics.

**Structure of the lithium solvation shell.** Next, we investigate the structure of the lithium solvation shell as a function of  $\chi_{\text{EC}}$ . First, we calculate the cumulative coordination number  $n(r)$  defined as

$$n(r) \equiv 4\pi\rho \int_0^r r'^2 g(r') dr', \quad (3)$$

where  $g(r)$  is the radial distribution function (RDF). In Fig. 3(a), we present  $n(r)$  of three components of the electrolyte as a function of distance  $r$  from a  $\text{Li}^+$  ion at the EC fraction of  $\chi_{\text{EC}} = 30\%$ . To calculate  $n(r)$ , we use the positions of the carbonyl oxygen  $\text{O}_c$  atom for EC and DMC and the P atom for  $\text{PF}_6^-$ . We find one plateau in  $n(r)$  for all three components, indicating that there is one solvation shell of a  $\text{Li}^+$  ion. We define the first plateau in  $n(r)$  as the first solvation shell of a  $\text{Li}^+$  ion and the value of  $n(r)$  at the first plateau as the solvation number  $N_c$  in the first solvation shell of a  $\text{Li}^+$  ion<sup>15</sup>. In Fig. 3(b), we present the solvation number  $N_c$  as a function of  $\chi_{\text{EC}}$ . As for  $\chi_{\text{EC}} = 10\%$ ,  $N_c^{\text{DMC}} (=2.60)$  is larger than  $N_c^{\text{EC}} (=0.92)$ , showing that a  $\text{Li}^+$  ion is solvated mostly by DMC. When  $\chi_{\text{EC}}$  further increases,  $N_c^{\text{EC}}$  increases and  $N_c^{\text{DMC}}$  decreases, resulting in that the majority of the first solvation shell of a  $\text{Li}^+$  ion becomes EC instead of DMC. We note that the total solvation number  $N_c^{\text{total}} (= N_c^{\text{PF}_6^-} + N_c^{\text{EC}} + N_c^{\text{DMC}})$  of the first solvation shell of a  $\text{Li}^+$  ion increases from  $N_c^{\text{total}} = 5.1$  at  $\chi_{\text{EC}} = 10\%$  to  $N_c^{\text{total}} = 5.6$  at  $\chi_{\text{EC}} = 60\%$ . Thus, as  $\chi_{\text{EC}}$  increases, the lithium-solvents complex becomes larger and heavier.

We further examine the structure between a  $\text{Li}^+$  ion and the two solvents. We calculate  $g_{\text{Li-O}_c}$  between a  $\text{Li}^+$  ion and the carbonyl oxygen atom  $\text{O}_c$  of EC and DMC<sup>33-35</sup>. The position of the first peak in  $g_{\text{Li-O}_c}$  is not influenced by the change in  $\chi_{\text{EC}}$ , but the intensity of the first peak decreases as  $\chi_{\text{EC}}$  increases. Even though the position of the first peak in  $g_{\text{Li-O}_c}$  does not change, the distribution of the  $\text{O}_c$  positions of EC and DMC in the lithium solvation

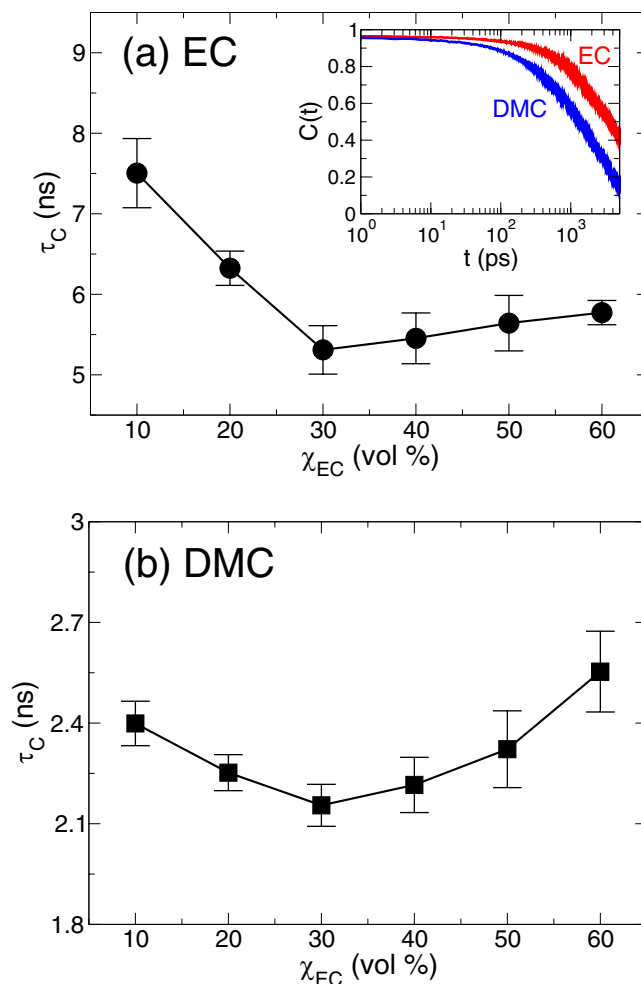


**Figure 2.** The exchange dynamics in the lithium solvation shell on a long time scale. The characteristic residence correlation times  $\tau_C$  of (a) EC and (b) DMC as a function of  $\chi_{EC}$ . Inset: the residence correlation time distributions  $C(t)$  of EC and DMC as a function of time  $t$  in a semi-log plot at the EC fraction of  $\chi_{EC} = 30\%$ .

shell could be affected by the change in  $\chi_{EC}$  due to the change in the shape of the first peak of  $g_{Li-O_c}$ . To see the effect of  $\chi_{EC}$  on a distance between solvents and a  $Li^+$  ion in the solvation shell, we further calculate the binding distance, that is, the average distance  $R_{avg}$  between a  $Li^+$  ion and the carbonyl oxygen atom  $O_c$  for EC and DMC within the first solvation shell of a  $Li^+$  ion. In Fig. 3(e), we present the average distance  $R_{avg}$  of EC and DMC as a function of  $\chi_{EC}$ . It shows that EC is generally located to a  $Li^+$  ion closer than DMC. For all  $\chi_{EC}$ s,  $R_{avg}^{EC}$  is smaller than  $R_{avg}^{DMC}$  by the same value of  $\Delta R_{avg} (\equiv R_{avg}^{DMC} - R_{avg}^{EC}) \sim 0.04 \text{ \AA}$ . Even though this difference in  $\Delta R_{avg}$  is too small, it appears consistently over the whole range of  $\chi_{EC}$  we investigated. As  $\chi_{EC}$  increases, both  $R_{avg}^{EC}$  and  $R_{avg}^{DMC}$  gradually increase. It indicates the increasing size of the first solvation shell of a  $Li^+$  ion with the increasing  $\chi_{EC}$ , which is directly related with the increasing size of the lithium-solvents complex. We find that the average position  $R_{avg}^{PF_6^-}$  of a  $PF_6^-$  ion in the first solvation shell of a  $Li^+$  ion shows a non-monotonic behavior with respect to  $\chi_{EC}$ . Figure 3(f) shows the minimum in  $R_{avg}^{PF_6^-}$  around  $\chi_{EC} = 30\%$ .

In addition to the average binding distance of the solvents, we consider the binding direction of EC and DMC with a  $Li^+$  ion to fully understand the nature of the lithium solvation structure as a function of  $\chi_{EC}$ <sup>36</sup>. Specifically, we investigate the distribution  $P(\theta)$  of a binding angle  $\theta$  between a  $Li^+$  ion and the carbonyl group of EC and DMC for various  $\chi_{EC}$ s. Here we consider an angle  $\theta \equiv \angle Li^+ O_c C$ , where  $O_c = C$  is the carbonyl group of EC and DMC. In Fig. 4(a,b), we present  $P(\theta)$  of EC and DMC. For EC, the maximum value in  $P(\theta)$  occurs at  $\theta_{EC}^{max} \simeq 156^\circ$  at  $\chi_{EC} = 10\%$  and it gradually decreases to  $\theta_{EC}^{max} \simeq 152^\circ$  at  $\chi_{EC} = 60\%$ . For DMC, the maximum occurs at  $\theta_{DMC}^{max} \simeq 158^\circ$  at  $\chi_{EC} = 10\%$  and it seems not to change upon increasing  $\chi_{EC}$ . For both solvents, the three atoms of Li,  $O_c$  and C tend to be slightly off a straight line<sup>25,37,38</sup>. Whereas  $P_{EC}(\theta)$  shows a shift toward the smaller angle upon changing  $\chi_{EC}$ ,  $P_{DMC}(\theta)$  for all  $\chi_{EC}$ s does not change the shape of the curve. From the calculation of the average angle,  $\langle \theta \rangle [\equiv \int \theta P(\theta) d\theta / \int P(\theta) d\theta]$ , we find that  $\langle \theta_{EC} \rangle$  decreases upon increasing  $\chi_{EC}$ . In contrast,  $\langle \theta_{DMC} \rangle$  is relatively insensitive to a change in  $\chi_{EC}$ . Note that the change  $\Delta \langle \theta_{EC} \rangle$  in the average angle is quite small ( $\Delta \langle \theta_{EC} \rangle \sim 1.9^\circ$  between  $\chi_{EC} = 10\%$  and  $60\%$ ).

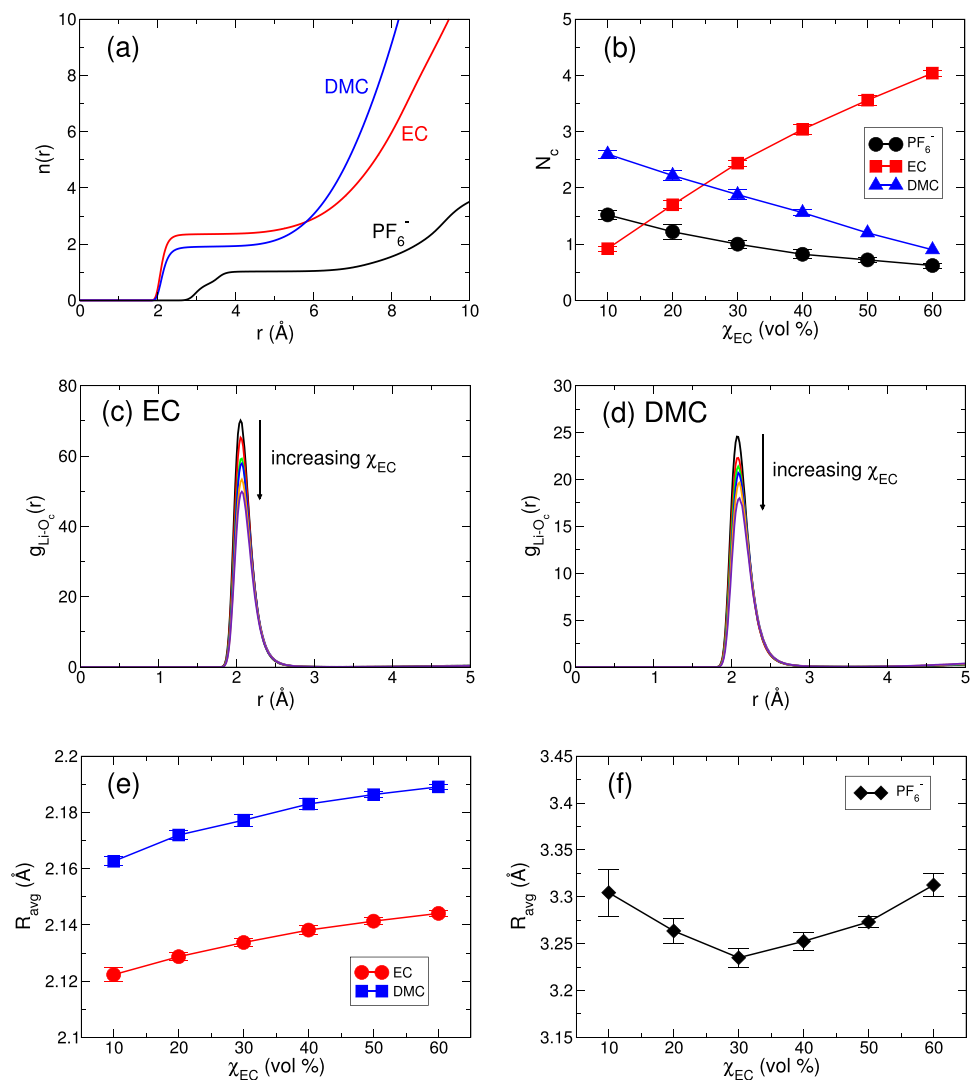


**Figure 3.** The structure of the first solvation shell of a  $\text{Li}^+$  ion. **(a)** The cumulative coordination number  $n(r)$  as a function of distance  $r$  at the EC fraction of  $\chi_{\text{EC}} = 30\%$ . **(b)** The solvation number  $N_c$  in the first solvation shell of a  $\text{Li}^+$  ion. The radial distribution function  $g_{\text{Li}^+-\text{O}_c}$  between a  $\text{Li}^+$  ion and a carbonyl oxygen atom of **(c)** EC and **(d)** DMC as a function of distance  $r$ . The first peak in  $g_{\text{Li}^+-\text{O}_c}$  is positioned at  $r = 2.06 \text{ \AA}$  for EC and  $2.09 \text{ \AA}$  for DMC, respectively. **(e)** The average distance  $R_{\text{avg}}$  of the carbonyl oxygen atom from a  $\text{Li}^+$  ion in the first solvation shell for EC and DMC as a function of  $\chi_{\text{EC}}$ , respectively. **(f)** The average distance  $R_{\text{avg}}$  of the phosphorus atom of  $\text{PF}_6^-$  from a  $\text{Li}^+$  ion as a function of  $\chi_{\text{EC}}$ .

**The translational and rotational dynamics of solvents.** To examine how the solvation dynamics of a  $\text{Li}^+$  ion is related with the motions of solvents, we consider the translational and rotational dynamics of EC and DMC. For the translational motion, we calculate the translational mean square displacement (TMSD)<sup>15,28,29,39–42</sup>,

$$\langle \Delta \vec{r}^2(t) \rangle \equiv \left\langle \frac{1}{N} \sum_{i=1}^N [\vec{r}_i(t) - \vec{r}_i(0)]^2 \right\rangle. \quad (4)$$

From the TMSD, we can calculate the translational diffusion constant  $D_T$  via the relation of

$$2dD_T t = \lim_{t \rightarrow \infty} \langle \Delta \vec{r}^2(t) \rangle, \quad (5)$$

where  $d$  is the dimensionality of the system. To obtain an expression of the rotational mean square displacement (RMSD)<sup>28,43</sup>, we first define the vector  $\vec{H}(t) \equiv \text{CO}_c$  of the carbonyl group of EC and DMC. For a time interval  $\delta t$ , the vector  $\vec{H}$  spans the angle  $\delta\varphi \equiv \cos^{-1}[\vec{H}(t + \delta t) \cdot \vec{H}(t)]$ . An angle vector  $\delta\vec{\phi}$  is to be that the magnitude is  $|\delta\vec{\phi}(t)| \equiv \delta\varphi$  and the direction is given by  $\vec{H}(t) \times \vec{H}(t + \delta t)$ . Finally, we obtain the angle vector  $\vec{\phi}(t)$  by summing  $\delta\vec{\omega}(t) (\equiv \delta\vec{\phi}(t)/\delta t)$  over time  $t$ ,

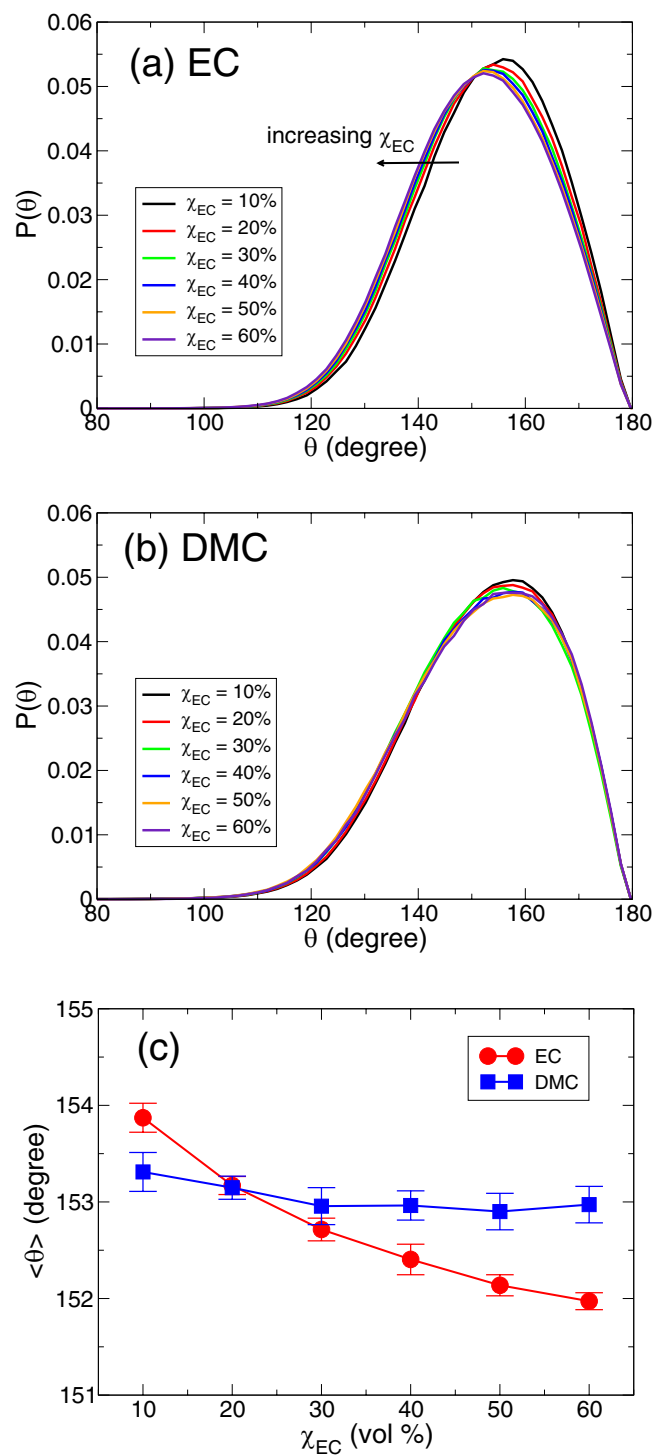


**Figure 4.** The binding direction of solvents with a  $\text{Li}^+$  ion. The angle distribution  $P(\theta)$  for (a) EC and (b) DMC. (c) The averaged value  $\langle \theta \rangle$  of an angle  $\theta$  between  $\text{Li}^+ \dots \text{O}_c$  and  $\text{O}_c=\text{C}$  of the carbonyl group of EC and DMC as a function of  $\chi_{EC}$ .

$$\vec{\phi}(t) = \int_0^t dt' \delta \vec{\omega}(t'). \quad (6)$$

Now we are able to define the RMSD similar to the TMSD,

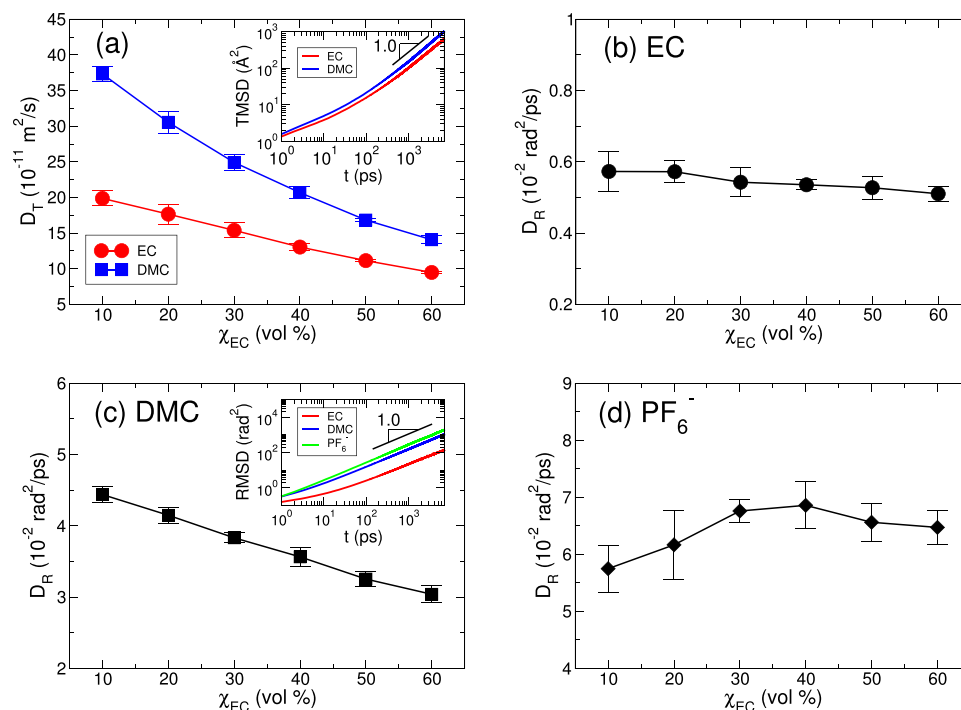


**Figure 5.** The translational and rotational diffusion constants. **(a)** The translational diffusion constants  $D_T$  of EC and DMC as a function of  $\chi_{EC}$ . Inset: the translational mean square displacements (TMSDs) of EC and DMC at  $\chi_{EC} = 30\%$  in a log-log plot, showing the diffusive regime (TMSD  $\propto t$ ) in the long time limit. The rotational diffusion constants  $D_R$  of **(b)** EC, **(c)** DMC and **(d)**  $PF_6^-$  as a function of  $\chi_{EC}$ . To calculate  $D_R$ , we use a vector connecting the carbon atom with the oxygen atom in the carbonyl group ( $C=O_c$ ) for both EC and DMC. Inset in **(c)**: the rotational mean square displacements (RMSDs) of EC, DMC and  $PF_6^-$  at  $\chi_{EC} = 30\%$  in a log-log plot, showing the diffusive regime (RMSD  $\propto t$ ) in the long time limit.

$$\langle \Delta \vec{\phi}^2(t) \rangle \equiv \left\langle \frac{1}{N} \sum_{i=1}^N [\vec{\phi}_i(t) - \vec{\phi}_i(0)]^2 \right\rangle. \quad (7)$$

From the RMSD, we similarly calculate the rotational diffusion constant  $D_R$  via the relation<sup>28,43</sup> of

$$4D_R t = \lim_{t \rightarrow \infty} \langle \Delta \vec{\phi}^2(t) \rangle. \quad (8)$$

In Fig. 5, we present the translational diffusion constant  $D_T$  and the rotational diffusion constant  $D_R$  of EC and DMC as a function of  $\chi_{EC}$ . For the translational dynamics, both  $D_T^{EC}$  and  $D_T^{DMC}$  monotonically decrease as  $\chi_{EC}$  increases<sup>23,44</sup>. Since EC has the much larger dielectric constant  $\varepsilon$  than DMC, the increase in  $\chi_{EC}$  entails the increase in the viscosity of the electrolyte, so that the translational dynamics in the electrolyte becomes slower<sup>1,5,15,45</sup>. On the other hand, the rotational dynamics of EC, DMC and  $PF_6^-$  is different from the translational dynamics in terms of  $\chi_{EC}$ . In Fig. 5(b and c), we present  $D_R^{EC}$  and  $D_R^{DMC}$  as a function of  $\chi_{EC}$ .  $D_R^{DMC}$  decreases upon increasing  $\chi_{EC}$ , but  $D_R^{EC}$  shows a behavior nearly insensitive to  $\chi_{EC}$ . For EC, a difference in  $D_R^{EC}$  between  $\chi_{EC} = 10\%$  and  $60\%$  is  $\Delta D_R^{EC} \sim 0.1 \times 10^{-2}$  (rad<sup>2</sup>/ps). For DMC,  $\Delta D_R^{DMC}$  is around  $1.5 \times 10^{-2}$  (rad<sup>2</sup>/ps), indicating that the effect of  $\chi_{EC}$  on the rotational dynamics of EC is very weak. The difference in the rotational dynamics of EC and DMC comes from various factors. As mentioned before, the dielectric constant  $\varepsilon$  of EC ( $\varepsilon \sim 90$  at  $40^\circ$ ) is much larger than DMC ( $\varepsilon \sim 3.1$  at  $25^\circ$ ), so that it causes the bigger drag against a rotational motion for EC than DMC. The carbonyl oxygen atom  $O_c$  of EC and DMC forms a bond with a  $Li^+$  ion but the intensity of the bonding is different for EC and DMC. As shown in Figs 1 and 2, the residence time of EC within the lithium solvation shell is always longer than DMC on both short and long time scales. It causes the more drag against the rotational motion of EC than DMC. In addition, the molecular structures of EC and DMC also cause the difference in the rotational dynamics such that the carbonyl group of EC needs more energy to rotate than one of DMC, because the moment of inertia about the rotational axis of EC is bigger than DMC. Those conditions result in the fact that the rotational dynamics of EC is slower than DMC by a factor of 7~8.

The rotational dynamics of a  $PF_6^-$  ion exhibits an interesting feature, as shown in Fig. 5(d). Due to the strong Coulombic interaction between cations and anions, the translational dynamics of  $PF_6^-$  is known to be much slower than EC and DMC<sup>15</sup>. Even though the residence time of  $PF_6^-$  in the first solvation shell of a  $Li^+$  ion is much longer than EC and DMC on both short and long time scales, we find that the rotational diffusion constant  $D_R^{PF_6^-}$

of  $\text{PF}_6^-$  is surprisingly larger than  $D_R^{\text{EC}}$  and  $D_R^{\text{DMC}}$ , indicating the faster rotational dynamics of  $\text{PF}_6^-$  than EC and DMC. This fast rotation of a  $\text{PF}_6^-$  ion is ascribed to the fact that a  $\text{PF}_6^-$  ion has six F atoms and each F atom tends to form a bond with a  $\text{Li}^+$  ion. It causes the reduction in the energy barrier needed to be overcome for the rotation within the solvation shell of a  $\text{Li}^+$  ion. The slow translational motion and fast rotational motion of  $\text{PF}_6^-$  indicate that a bonding of one F atom of  $\text{PF}_6^-$  with  $\text{Li}^+$  remains for short time and is replaced by one of the other F atoms of the same  $\text{PF}_6^-$  ion.

## Conclusion

The lithium solvation structure and dynamics are of great importance to understand lithium ion batteries. It is known that the formation of the SEI on the electrode is significantly affected by the solvation structure of a  $\text{Li}^+$  ion, since the most contribution to the SEI is ascribed to the decomposition of the solvents in the solvation shell of a  $\text{Li}^+$  ion near the electrode<sup>17</sup>. Thus, the information of the primary solvation structure of a  $\text{Li}^+$  ion is critical for the performance of lithium ion batteries and many research has studied the solvation structure in nonaqueous electrolytes with binary or ternary solvents<sup>9,17,46</sup>. In addition, the solvation dynamics can greatly affect the mobility of a  $\text{Li}^+$  ion<sup>15</sup>. The faster exchange dynamics of solvents in the solvation shell invokes the weaker rigidity of the lithium solvation shell. The solvation structure and dynamics are strongly correlated in such a way that the exchange dynamics in the lithium solvation shell is affected by the solvent composition of the shell<sup>27</sup>. However, the relation between the solvation structure and the exchange dynamics is far from being fully understood.

In this work, we have performed molecular dynamics simulations to investigate the dynamical properties of nonaqueous electrolytes as a function of the mixture ratio of binary solvents. We have found that the exchange dynamics of EC and DMC in the lithium solvation shell shows a non-monotonic behavior on a short time scale with respect to  $\chi_{\text{EC}}$ . It indicates that the response of the rigidity of the solvation shell to the thermal fluctuation is different according to the composition of the shell and the response does not change monotonically with the increasing number of EC in the solvation shell. We have further found that this non-monotonic behavior on a short time scale keeps preserved on a long time scale. As  $\chi_{\text{EC}}$  increases, the average distances of EC and DMC from a  $\text{Li}^+$  ion increase, so that the two solvents move toward the boundary of the lithium solvation shell. However, the diffusion of both solvents slows down due to the increase in the viscosity. Thus, with a given size of the lithium solvation shell, it seems that the resulting exchange dynamics of two solvents is ascribed to a competition between the location of solvents in the solvation shell and the motion of them. Furthermore, our results show that the binding angle of DMC to a  $\text{Li}^+$  ion seems to be insensitive to a change in  $\chi_{\text{EC}}$ , whereas the binding angle of EC gradually decreases upon increasing  $\chi_{\text{EC}}$ . The rotational dynamics of EC shows a different dependences in magnitude of  $D_R$  on  $\chi_{\text{EC}}$  compared to the rotational dynamics of DMC. We note that a  $\text{PF}_6^-$  ion presents many interesting features in structure and dynamics. The average distance from a  $\text{Li}^+$  ion shows a minimum around at  $\chi_{\text{EC}} = 30\%$  different from EC and DMC. The rotational dynamics of  $\text{PF}_6^-$  is faster than EC and DMC, whereas the translational dynamics of it is the slowest. Finally, we believe that our results will give valuable insights to broaden our understanding of nonaqueous electrolytes of lithium ion batteries.

## Methods

We perform molecular dynamics (MD) simulations of nonaqueous electrolytes of lithium ion batteries consisting of a solution of 1M lithium hexafluorophosphate ( $\text{LiPF}_6$ ) salt in a binary solvent mixture of ethylene carbonate (EC) and dimethyl carbonate (DMC). We carry out all simulations using the MD simulation package, LAMMPS<sup>47</sup>. We implement the OPLS/AA force field to describe the molecular interaction of the solvents<sup>15,48</sup>. We compute the long-range interactions using particle-particle particle-mesh (PPPM) algorithm. For the non-bonded interaction, we use the Lennard-Jones interaction with a cutoff of 10 Å. We use the combination rule of Lorentz-Berthelot for the intermolecular interactions. We perform the simulations in the *NVT* ensemble, where *N*, *V* and *T* are the number of molecules, the volume, and the temperature, respectively. For salt, we use  $N_{\text{salt}} = 176$ . For solvents, we use  $N_{\text{EC}} = 264 \sim 1584$  and  $N_{\text{DMC}} = 832 \sim 1872$  depending on the EC fraction and use  $L = 6.7108$  nm as the linear size of the simulation box, which gives the similar density to the experimental density<sup>49</sup>. We keep the temperature constant via the Nöse-Hoover thermostat with a time constant of 0.1 ps during the simulations. We equilibrate the system for  $t = 40$  ns and collect the data for additional time  $t = 6$  ns for each 1 ps timestep. We apply periodic boundary conditions in all three directions of the simulation box. We use  $\Delta t = 1$  fs as a timestep of the simulation. We investigate electrolytes in a range of the solvent mixture ratios from EC:DMC = 10%:90% up to 60%:40% (in volume %). We run 25 independent simulations to collect trajectories for improving the statistics. All averages and the sample standard deviations (error bars) in the figures are calculated from 25 independent datasets.

## Data Availability

The datasets generated during and/or analysed during the current study are available from the corresponding author on reasonable request.

## References

- Xu, K. Nonaqueous liquid electrolytes for lithium-based rechargeable batteries. *Chem. Rev.* **104**, 4303–4417 (2004).
- Aurbach, D. *et al.* Design of electrolyte solutions for Li and Li-ion batteries: a review. *Electrochim. Acta* **50**, 247–254 (2004).
- Goodenough, J. B. & Kim, Y. Challenges for rechargeable Li batteries. *Chem. Mater.* **22**, 587–603 (2010).
- Etacheri, V. *et al.* Challenges in the development of advanced Li-ion batteries: a review. *Energy Environ. Sci.* **4**, 3243–3262 (2011).
- Xu, K. Electrolytes and interphases in Li-ion batteries and beyond. *Chem. Rev.* **114**, 11503–11618 (2014).
- Postupna, O. O., Kolesnik, Y. V., Kalugin, O. N. & Prezhdov, O. V. Microscopic structure and dynamics of  $\text{LiBF}_4$  solutions in cyclic and linear carbonates. *J. Phys. Chem. B* **115**, 14563–14571 (2011).
- Kumar, N. & Seminario, J. M. Lithium-ion model behavior in an ethylene carbonate electrolyte using molecular dynamics. *J. Phys. Chem. C* **120**, 16322–16332 (2016).



8. Yang, L., Xiao, A. & Lucht, B. L. Investigation of solvation in lithium ion battery electrolytes by NMR spectroscopy. *J. Mol. Liq.* **154**, 131–133 (2010).
9. von Wald Cresce, A., Borodin, O. & Xu, K. Correlating Li<sup>+</sup> solvation sheath structure with interphasial chemistry on graphite. *J. Phys. Chem. C* **116**, 26111–26117 (2012).
10. Bogle, X. *et al.* Understanding Li<sup>+</sup>-solvent interaction in nonaqueous carbonate electrolyte with <sup>17</sup>O NMR. *J. Phys. Chem. Lett.* **4**, 1664–1668 (2013).
11. Skarmoutsos, I., Ponnuchamy, V., Vetere, V. & Mossa, S. Li<sup>+</sup> solvation in pure, binary, ternary mixtures of organic carbonate electrolytes. *J. Phys. Chem. C* **119**, 4502–4515 (2015).
12. Giorgini, M. G. *et al.* Solvation structure around the Li<sup>+</sup> ion in mixed cyclic/linear carbonate solutions unveiled by Raman noncoincidence effect. *J. Phys. Chem. Lett.* **6**, 3296–3302 (2015).
13. Borodin, O. *et al.* Competitive lithium solvation of linear and cyclic carbonates from quantum chemistry. *Phys. Chem. Chem. Phys.* **18**, 164–175 (2016).
14. Cui, W. *et al.* Lithium ion solvation by ethylene carbonates in lithium-ion battery electrolytes, revisited by density functional theory with the hybrid solvation model and free energy correction in solution. *Phys. Chem. Chem. Phys.* **18**, 23607–23612 (2016).
15. Han, S. A salient effect of density on the dynamics of nonaqueous electrolytes. *Sci. Rep.* **7**, 46718 (2017).
16. Xu, K. *et al.* Solvation sheath of Li<sup>+</sup> in nonaqueous electrolytes and its implication of graphite/electrolyte interface chemistry. *J. Phys. Chem. C* **111**, 7411–7421 (2007).
17. Xu, K. Charge-transfer process at graphite/electrolyte interface and the solvation sheath structure of Li<sup>+</sup> in nonaqueous electrolytes. *J. Electrochem. Soc.* **154**, A162–A167 (2007).
18. Nie, M. *et al.* Role of solution structure in solid electrolyte interphase formation on graphite with LiPF<sub>6</sub> in propylene carbonate. *J. Phys. Chem. C* **117**, 25381–25389 (2013).
19. Ding, M. S. *et al.* Change of conductivity with salt content, solvent composition, and temperature for electrolytes of LiPF<sub>6</sub> in ethylene carbonate-ethyl methyl carbonate. *J. Electrochem. Soc.* **148**, A1196–A1204 (2001).
20. Morita, M., Asai, Y., Yoshimoto, N. & Ishikawa, M. A Raman spectroscopic study of organic electrolyte solutions based on binary solvent systems of ethylene carbonate with low viscosity solvents which dissolve different lithium salts. *J. Chem. Soc. Faraday Trans.* **94**, 3451–3456 (1998).
21. Kondo, K. *et al.* Conductivity and solvation of Li<sup>+</sup> ions of LiPF<sub>6</sub> in propylene carbonate solutions. *J. Phys. Chem. B* **104**, 5040–5044 (2000).
22. Kameda, Y. *et al.* Solvation structure of Li<sup>+</sup> in concentrated LiPF<sub>6</sub> - propylene carbonate solutions. *J. Phys. Chem. B* **111**, 6104–6109 (2007).
23. Hayamizu, K. Temperature dependence of self-diffusion coefficients of ions and solvents in ethylene carbonate, propylene carbonate, and diethyl carbonate single solutions and ethylene carbonate + diethyl carbonate binary solutions of LiPF<sub>6</sub> studied by NMR. *J. Chem. Eng. Data* **57**, 2012–2017 (2012).
24. Seo, D. M. *et al.* Role of mixed solvation and ion pairing in the solution structure of lithium ion battery electrolytes. *J. Phys. Chem. C* **119**, 14038–14046 (2015).
25. Ong, M. T. *et al.* Lithium ion solvation and diffusion in bulk organic electrolytes from first-principle and classical reactive molecular dynamics. *J. Phys. Chem. B* **119**, 1535–1545 (2015).
26. Tang, Z.-K., Tse, J. S. & Liu, L.-M. Unusual Li-ion transfer mechanism in liquid electrolytes: a first-principles study. *J. Phys. Chem. Lett.* **7**, 4795–4801 (2016).
27. Liang, C., Kwak, K. & Cho, M. Revealing the solvation structure and dynamics of carbonate electrolytes in lithium-ion batteries by two-dimensional infrared spectrum modeling. *J. Phys. Chem. Lett.* **8**, 5779–5784 (2017).
28. Han, S. Dynamic features of water molecules in superconcentrated aqueous electrolytes. *Sci. Rep.* **8**, 9347 (2018).
29. Han, S. Anionic effects on the structure and dynamics of water in superconcentrated aqueous electrolytes. *RSC Adv.* **9**, 609–619 (2019).
30. Han, S., Kumar, P. & Stanley, H. E. Hydrogen-bond dynamics of water in a quasi-two-dimensional hydrophobic nanopore slit. *Phys. Rev. E* **79**, 041202 (2009).
31. Lee, K.-K. *et al.* Ultrafast fluxional exchange dynamics in electrolyte solvation sheath of lithium ion battery. *Nat. Commun.* **8**, 14658 (2017).
32. Fulfer, K. D. & Kuroda, D. G. Solvation structure and dynamics of the lithium ion in organic carbonate-based electrolytes: a time-dependent infrared spectroscopy study. *J. Phys. Chem. C* **120**, 24011–24022 (2016).
33. Soetens, J.-C., Millot, C., Maigret, B. & Bakó, I. Molecular dynamics simulation and X-ray diffraction studies of ethylene carbonate, propylene carbonate and dimethyl carbonate in liquid phase. *J. Mol. Liq.* **92**, 201–216 (2001).
34. Borodin, O. & Smith, G. D. Quantum chemistry and molecular dynamics simulation study of dimethyl carbonate: ethylene carbonate electrolyte doped with LiPF<sub>6</sub>. *J. Phys. Chem. B* **113**, 1763–1776 (2009).
35. Jorn, R., Kumar, R., Abraham, D. P. & Voth, G. A. Atomistic modeling of the electrode-electrolyte interface in Li-ion energy storage systems: electrolyte structuring. *J. Phys. Chem. C* **117**, 3747–3761 (2013).
36. Fulfer, K. D. & Kuroda, D. G. A comparison of the solvation structure and dynamics of the lithium ion in linear organic carbonates with different alkyl chain lengths. *Phys. Chem. Chem. Phys.* **19**, 25140–25150 (2017).
37. Masia, M., Probst, M. & Rey, R. Ethylene carbonate - Li<sup>+</sup>: a theoretical study of structural and vibrational properties in gas and liquid phases. *J. Phys. Chem. B* **108**, 2016–2027 (2004).
38. Ganesh, P., Jiang, D. & Kent, P. R. C. Accurate static and dynamic properties of liquid electrolytes for Li-ion batteries from ab initio molecular dynamics. *J. Phys. Chem. B* **115**, 3085–3090 (2011).
39. Han, S., Kumar, P. & Stanley, H. E. Absence of a diffusion anomaly of water in the direction perpendicular to hydrophobic nanoconfining walls. *Phys. Rev. E* **77**, 030201 (2008).
40. Han, S., Choi, M. Y., Kumar, P. & Stanley, H. E. Phase transitions in confined water nanofilms. *Nat. Phys.* **6**, 685–689 (2010).
41. Han, S. Anomalous change in the dynamics of a supercritical fluid. *Phys. Rev. E* **84**, 051204 (2011).
42. Ong, M. T. *et al.* Complex ion dynamics in carbonate lithium-ion battery electrolytes. *J. Phys. Chem. C* **121**, 6589–6595 (2017).
43. Kämmerer, S., Kob, W. & Schilling, R. Dynamics of the rotational degrees of freedom in a supercooled liquid of diatomic molecules. *Phys. Rev. E* **56**, 5450–5461 (1997).
44. Tenney, C. M. & Cygan, R. T. Analysis of molecular clusters in simulations of lithium-ion battery electrolytes. *J. Phys. Chem. C* **117**, 24673–24684 (2013).
45. Zwanzig, R. On the relation between self-diffusion and viscosity of liquids. *J. Chem. Phys.* **79**, 4507–4508 (1983).
46. Borodin, O. & Bedrov, D. Interfacial structure and dynamics of the lithium alkyl dicarbonate SEI components in contact with the lithium battery electrolyte. *J. Phys. Chem. C* **118**, 18362–18371 (2014).
47. Plimpton, S. J. Fast parallel algorithms for short-range molecular dynamics. *J. Comp. Phys.* **117**, 1–19 (1995).
48. You, X., Chaudhari, M. I., Rempe, S. B. & Pratt, L. R. Dielectric relaxation of ethylene carbonate and propylene carbonate from molecular dynamics simulations. *J. Phys. Chem. B* **120**, 1849–1853 (2016).
49. Porion, P. *et al.* Comparative study on transport properties for LiFAP and LiPF<sub>6</sub> in alkyl-carbonates as electrolytes through conductivity, viscosity and NMR self-diffusion measurements. *Electrochim. Acta* **114**, 95–104 (2013).

### Author Contributions

S.H. designed the research; carried out simulations; analysed data and wrote the paper.

### Additional Information

**Competing Interests:** The author declares no competing interests.

**Publisher's note:** Springer Nature remains neutral with regard to jurisdictional claims in published maps and institutional affiliations.



**Open Access** This article is licensed under a Creative Commons Attribution 4.0 International License, which permits use, sharing, adaptation, distribution and reproduction in any medium or format, as long as you give appropriate credit to the original author(s) and the source, provide a link to the Creative Commons license, and indicate if changes were made. The images or other third party material in this article are included in the article's Creative Commons license, unless indicated otherwise in a credit line to the material. If material is not included in the article's Creative Commons license and your intended use is not permitted by statutory regulation or exceeds the permitted use, you will need to obtain permission directly from the copyright holder. To view a copy of this license, visit <http://creativecommons.org/licenses/by/4.0/>.

© The Author(s) 2019